Journal of Physics and Chemistry of Solids 187 (2024) 111860

Contents lists available at ScienceDirect

Journal of Physics and Chemistry of Solids

journal homepage: www.elsevier.com/locate/jpcs

Thermal expansion of 4H and 6H SiC from 5 K to 340 K

J.J. Neumeier [a,*], Yu.V. Shvyd'ko [b], D. Haskel [b]

[a] Physics Department, Montana State University, Bozeman, MT 59717-3840, USA
[b] Advanced Photon Source, Argonne National Laboratory, Argonne, IL 60439, USA

ARTICLE INFO

Keywords:
Thermal expansion
Coefficient
Thermal properties
Structural properties
Silicon carbide

ABSTRACT

The first thermal expansion measurements of the 4H and 6H polytypes of SiC below room temperature are reported. The measurements were carried out on single-crystal specimens using high-resolution capacitive-based dilatometry. For both polytypes, the thermal expansion coefficient is below 2.4×10^{-6} 1/K near room temperature. No phase transitions are observed over the 5 K to 340 K temperature range of the measurements. The thermal expansion coefficient α of 4H SiC is slightly anisotropic for measurements parallel and perpendicular to the crystallographic c axis with $\alpha^{||}$ about 2.2×10^{-7} 1/K larger than $\alpha^{\perp}$ near room temperature. For 6H SiC no discernible anisotropy is observed. The differences in anisotropy can be understood by considering the ratio of hexagonal to cubic bonds of each polytype. Narrow regions with negative thermal expansion that are within the limits of our resolution ($\sim 1 \times 10^{-8}$) are observed in the vicinity of 30 K for both specimens. Tabulated data, polynomial fits, fit parameters, and comparison to data based on lattice-parameter measurements are provided.

1. Introduction

Silicon Carbide (SiC) is an important material from a technological standpoint for both its electronic [1] and mechanical properties [2]. It is used widely as an abrasive, in the production of hard, durable tools, parts for automobiles, filtration, armor [3], advanced composite materials [4], and nuclear-fuel coatings [5]. It is also used for electrical/electronic applications such as furnace heating elements, and as a component in diodes, transistors, LEDs, single-photon sources, and pyrometers. Its low thermal expansion coefficient and high reflectivity make it an ideal material for construction of telescope mirrors [6,7]. Recently, coherent control of defect spin qubits in 4H SiC has been demonstrated [8,9] at 300 K, making it a host material for quantum computing platforms.

In this communication, the thermal expansions of the 4H and 6H polytypes of single crystalline SiC are reported for the temperature range 5 K < T < 340 K for the first time. The thermal expansion coefficient is a fundamental thermodynamic quantity of a material, on par with the magnetization, specific heat, and compressibility. It can be important for developing a fundamental understanding of a solid, and also for a broad array of engineering needs. We embarked on these measurements because the data were necessary for evaluation of SiC for optimal integration of SiC crystals for the new beamline POLAR, of the upgraded Advanced Photon Source at Argonne National Laboratory. There, cryogenically cooled 6H-SiC crystals alongside commonly used Si(111) crystals will be integrated into a vertically-diffracting double-crystal monochromator, in order to preserve a high degree of circular polarization and reduce intensity suppression of linear vertical polarization delivered by polarizing undulators in the tender energy range around 2.8 keV, where Si(111) diffracts near 45 degrees [10].

Prior determination of the linear thermal expansions and thermal expansion coefficients for SiC from room temperature to 1273 K [11–13] involved measurements of the lattice parameters determined from x-ray diffraction data. The present work uses capacitive-based dilatometry, which is able to discern changes in sample length of 1 part in 10^8, for a relative resolution [14] in determining length changes exceeding that of lattice parameter measurements by a factor of 10^3 to 10^4. This work also extends the temperature range to 5 K, allows comparison to the data from lattice parameter measurements near room temperature, and is able to reliably address anisotropy and regions of negative thermal expansion. The data presented here will serve as a testbed for calculations [15,16] of the thermal expansion of SiC and it will be useful for calculations that require the thermal expansion as an input [17]. Furthermore, they will provide significant improvement in the knowledge of lattice mismatch between SiC substrates and epitaxial thin films deposited on them [18] for the benefit of predictions regarding the performance of advanced devices relying on SiC substrates.

* Corresponding author.
E-mail address: neumeier@montana.edu (J.J. Neumeier).

https://doi.org/10.1016/j.jpcs.2023.111860
Received 19 September 2023; Received in revised form 9 November 2023; Accepted 22 December 2023
Available online 27 December 2023

2. Experimental and data analysis

The thermal expansion of 4H and 6H SiC was measured using a capacitive-based dilatometer cell constructed of fused silica [14]. The dilatometer cell is designed so that a change in sample length results in a change in the gap of a parallel-plate capacitor that is integral to the cell. A highly sensitive capacitance bridge allows capacitor gap changes of 0.1 Å to be resolved, making this the most sensitive method for measuring the thermal expansion of a solid. Fused silica possesses a very small thermal expansion coefficient compared to other materials that are typically used for the construction of dilatometer cells [19]. This is important, since the measurement actually determines the differential expansion between the sample and the material from which the dilatometer cell is constructed. Correction for the differential expansion must be made using published data. In this work, thermal expansion data of fused silica (NIST SRM 739) obtained using an absolute technique [20,21] were used. The data from Refs. [20,21] cover two different temperature regions, both of which were required. Those data were fitted to a cubic spline to provide values for our differential expansion corrections. The dilatometer cell was calibrated by measuring a specimen of high-purity copper and comparing to published results [22] which have an uncertainty in the thermal expansion coefficient of about 10^{-10} K^{-1}; the agreement of our linear thermal expansion data with theirs is within 0.1%. For a typical measurement, the specimen is mounted in the cell, the measurement chamber is evacuated, ~30 mbar of dry helium gas is admitted to the chamber, and the specimen is cooled to 5 K. Changes in specimen length ΔL of 0.1 Å can be resolved for a relative resolution of 1 part in 4×10^8 to 1.3×10^9 for the range of specimen lengths studied here (4 mm to 12.9 mm). Data are acquired on warming at a rate of 0.2 K/min. A complete description of the measurement apparatus can be found in Ref. [14].

Fig. 1 illustrates details regarding typical measurement data and analysis thereof. Panel (a) shows the raw capacitance C versus temperature T data, along with the same data corrected for the empty-cell (addenda) effect. The empty-cell effect is associated with changes in the capacitor plate area and gap, due to the expansion of fused-silica, as well as imperfections in the cell fabrication and other unknown effects. This small effect, estimated using the uncorrected and corrected values of C at 294 K and the cell's calibration factor, is equivalent to a change in capacitor gap of 175 nm, smaller than a wavelength of visible light. Fig. 1(b) shows the capacitor gap d calculated using the relation $d = \epsilon A/C$, where $\epsilon A = 1618.3$ μm pF is the calibration factor determined by measuring the copper standard. Correction for the differential expansion between fused-silica and the specimen [14] leads to the other curve shown in Fig. 1(b). The correction for this effect, in comparison to the thermal expansion of SiC, will be discussed below. Note that there are two temperatures where the correction is zero, due to fused silica's exhibition of positive and negative thermal expansion. The corrected data for d are used to calculate the linear thermal expansion from $\Delta L(T) = d(T) - d_{294}$, which is then normalized to the specimen length at 294 K to yield the data shown in the main panel of Fig. 1(c). Those data are then differentiated using a point-by-point derivative to yield $\alpha = \mathrm{d}(\Delta L/L_{294})/\mathrm{d}T$ (see inset). No smoothing has been done in any of the analysis. Note that the vertical scatter in α of ~10^{-8} K^{-1} is typical. It is mostly attributable to the resolution in the temperature channel that has at least 1000× poorer resolution than the capacitance channel. Variation in the heating rate plays a role too; normally it is controlled at ±0.001 K/min, but between 25 and 40 K rapid boil off of liquid helium causes the rate to stray well above, leading to additional scatter in α.

Although fused silica has among the smallest known thermal expansions between 30 K < T < 300 K, the thermal expansion of SiC is also small. To put this into perspective, based on the results to be presented below, at 300 K, α of SiC (α_{SiC}) is 4.9 times larger than α of fused silica (α_{SiO_2}). At 120 K, $|\alpha_{SiC}| = |\alpha_{SiO_2}|$, and by ~40 K $|\alpha_{SiO_2}|/|\alpha_{SiC}|$ reaches ≈ 28. Since the known thermal expansion of fused silica is used to correct for the differential expansion between fused-silica and the specimen, the uncertainties of the fused silica data [21], which are ~1×10^{-8} 1/K, is the main source of absolute uncertainty in the present study.

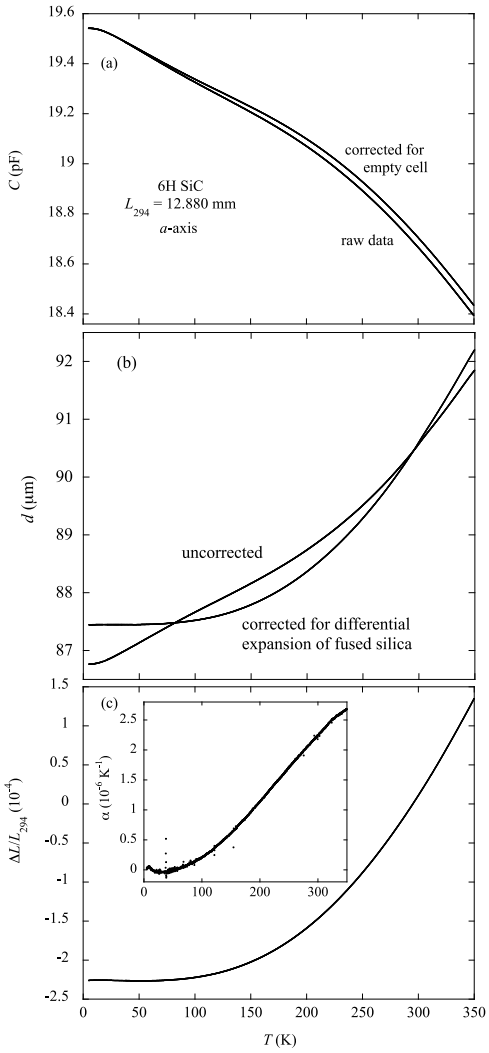

Fig. 1. (a) Capacitance versus temperature T data from measurements on a 6H SiC sample with length at 294 K, L_{294} = 12.880(1) mm. Data corrected for the empty-cell effect is shown. (b) Capacitor gap calculated from the corrected data in panel (a) using the relation $d = \epsilon A/C$. Data corrected for the differential expansion between fused-silica and the sample. (c) Main panel shows the linear thermal expansion $\Delta L/L_{294}$ versus T. The inset shows thermal expansion coefficient $\alpha = \mathrm{d}(\Delta L/L_{294})\mathrm{d}T$ using a point-by-point derivative.

The 4H-SiC specimen used herein was a semi-insulating type, 500(25) micron thick, 4 inch diameter wafer with the c-axis normal to the (0001) surface (±0.5° error). It was transparent, with no obvious color.[1] The wafer was wire cut into 5×5 mm^2 squares. The 6H-SiC crystal was grown using the Lely method by SICrystal AG (Eschenfelden, Germany). This crystal was deep green in color.

[1] The 4H-SiC crystal's manufacturer provided thermal conductivity values at 298 K of 4.9 and 3.9 W/cm-K for a and c axes, respectively, total dislocation density below 10^4 cm^{-2}, electrical resistivity > 10^7 Ω cm, and doping concentration (V-doped) ~5×10^{18} cm^{-3}. This is Zero MPD grade (less than 1/cm^{-2} Micropipe dislocations - i.e. hollow-core super screw dislocations with the Burgers vectors being multiple of the c lattice constant). The wafer was optically polished with Ra < 1 nm on the surface.

3. Thermal expansion of 4H SiC

A 4H SiC crystal with length perpendicular to c of 10.142(1) mm was measured at least twice along this direction. The crystal was only 0.5 mm thick parallel to c, so it was cut into 8 pieces, which were then stacked, yielding an overall length of 3.979(1) mm, and measured twice. The data were analyzed as discussed in Section 2. Following those steps, the resulting α data obtained via the point by point derivative of $\Delta L/L_{294}$ were combined into a single data file for each direction, and fitted using a third-order Chebyshev polynomial given by

$$\alpha(T) = A + BT + C(2T^2 - 1) + D(4T^3 - 3T). \quad (1)$$

In this fitting process, we add the data point $T = 0$ K, $\alpha = 0$, which is demanded by the third law of thermodynamics. The fit parameters are provided in the Appendix. The scatter about the fit was less than $\pm 2 \times 10^{-8}$. This fit was then integrated to yield the linear thermal expansion $\Delta L/L_0$, where the subscript denotes $T = 0$ K. The $\alpha(T)$ and the $\Delta L/L_0$ data so generated agreed well with the measured values. The $\alpha(T)$ and $\Delta L/L_0$ curves plotted in Fig. 2 are the result of this fitting process. The volume expansion $\Delta V/V_0$ was calculated from $\Delta V/V_0 = 2\Delta L_\perp/L_0 + \Delta L_\parallel/L_0$ and the volume expansion coefficient $\beta = \mathrm{d}\Delta V/V_0/\mathrm{d}T = 2\alpha_\perp + \alpha_\parallel$. The $\Delta L/L_0$, α, $\Delta V/V_0$, and β values are tabulated in the Appendix. Note that $\parallel$ and $\perp$ refer to the measurement directions relative to the c axis.

The data plotted in Fig. 2(a) illustrate upturns in $\alpha(T)$ on cooling below ~50 K for both directions and $\alpha^\parallel$ negative over a narrow temperature range. This type of behavior in $\alpha(T)$ generally indicates the dominance of some low-energy anharmonic phonons [23,24]. Since the third law of thermodynamics demands that $\alpha \to 0$ as $T \to 0$, one expects $\alpha(T)$ to bend toward zero below the lowest temperature of our measurements. 4H SiC exhibits some anisotropy for $\Delta L/L_0^\parallel$ and $\Delta L/L_0^\perp$. This leads to $\alpha^\parallel$ about 2×10^{-7} larger than $\alpha^\perp$ near room temperature. Below ~170 K $\alpha^\perp$ becomes larger than $\alpha^\parallel$, until about 20 K, where the trend reverses again.

4. Thermal expansion of 6H SiC

A 6H SiC crystal with length along the c-axis of 4.003(1) mm and length perpendicular to c of 12.880(1) mm was measured at least twice along each direction. The data were analyzed as discussed in Section 2. Following those steps, the resulting α data obtained via the point by point derivative of $\Delta L/L_{294}$ were combined into a single data file for each direction, and fitted using Eq. (1). The scatter about the fit was less than $\pm 2 \times 10^{-8}$. This fit was used to generate the curves plotted in Fig. 3(a). The fit parameters, $\Delta L/L_0$, α, $\Delta V/V_0$, and β values are tabulated in the Appendix. Note that the $L \parallel c$ data have been shifted upward by 0.1×10^{-6} 1/K so that the temperature dependence of both curves is visible, otherwise the curves lie directly on top of one another. The data were then integrated to yield the $\Delta L/L_0$ plotted in Fig. 3(b). In this case, the $\Delta L/L_0$ data have been shifted upward by 10×10^{-6} for clarity. Notable is the lack of anisotropy between the α values for $L \perp c$ and $L \parallel c$, which is smaller than our resolution until $T > 300$ K, where $\alpha^\parallel$ exceeds $\alpha^\perp$ by about 1×10^{-8} 1/K. The lack of anisotropy observed is uncommon for hexagonal crystal structures [25]. The $\alpha^\perp$ data illustrate a region of negative thermal expansion from 10 K $< T <$ 50 K that is within our range of absolute resolution. The $\alpha^\parallel$ data illustrate a region of negative thermal expansion from 20 K $< T <$ 40 K that is weaker than that of $\alpha^\perp$, but outside of our range of absolute resolution. Given the lack of anisotropy between $\alpha^\perp$ and $\alpha^\parallel$, these differences in negative expansion might be associated with the longer length of the sample for the $\alpha^\perp$ measurement, which improves the resolution of the experiment. Most likely, negative thermal expansion occurs along both axes with comparable magnitude.

Similar to the thermal expansion of 4H SiC, the thermal expansion of 6H SiC is extremely small. The data plotted in Fig. 3(b) also illustrate an upturn in $\alpha(T)$ below 20 K. Since the third law of thermodynamics demands that $\alpha \to 0$ as $T \to 0$, one expects $\alpha(T)$ to bend toward zero below the lowest temperature of our measurements.

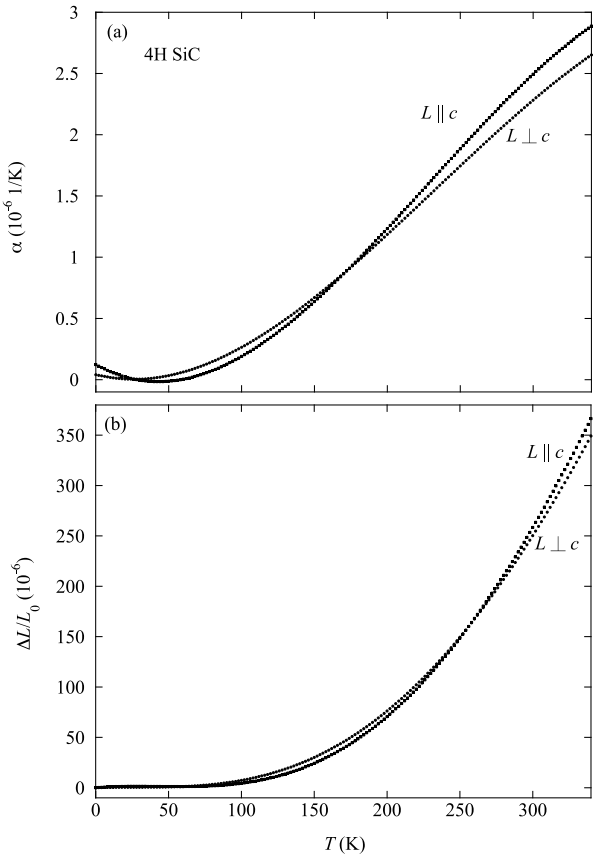

Fig. 2. Thermal expansion data for 4H SiC. (a) Thermal expansion coefficient α versus T. (b) Linear thermal expansion $\Delta L/L_0$ versus T.

5. Discussion

The 4H and 6H SiC $\alpha(T)$ data are compared to published results obtained from diffraction studies [11–13] in Fig. 4. Note that α_{11} corresponds to $\alpha_\perp$ ($L \perp c$) and α_{33} corresponds to $\alpha_\parallel$ ($L \parallel c$). For 4H SiC, the values of α_{11} and α_{33} and the slopes of α obtained from the diffraction studies are in poor agreement with one another. For 6H SiC, α_{11} is larger than α_{33} in one study [12], and the reverse is reported by the other [13]. The slopes from these two diffraction studies are in poor agreement too. Furthermore, the slopes of the data from Refs. [11,12] do not appear as if they would satisfy $\alpha \to 0$ as $T \to 0$, as demanded by the 3rd law of thermodynamics. This brief assessment, and comparison to the data presented herein, leads us to conclude that the thermal expansion coefficients reported in the three diffraction studies possess absolute uncertainties in the range of 1×10^{-6} 1/K or larger; no uncertainty estimates for α were stated for comparison to this estimate. The relative resolution of $\Delta L/L$ in the present measurements is 10^{-8} to 10^{-9}, which over a 10 K temperature range yields a relative resolution of 10^{-9} to 10^{-10} 1/K in α; this neglects the scatter shown in the inset of Fig. 1(c), which is largely associated with the point-by-point derivative obtained at 0.2 K intervals. Furthermore, the absolute resolution is about 1×10^{-8} 1/K. For these reasons, it is concluded that our α values are in agreement with those of Refs. [11–13] within the estimated uncertainties, but the present data possess a factor of 100 better absolute resolution.

Comparing our data further with those from diffraction studies, the c-axis lattice parameter data from Ref. [12] are plotted as $\Delta c/c_{294}$ along with the raw $\Delta L/L_{294}$ ($L \parallel c$) data from the present work in Fig. 5. Our plotted data set includes 1869 data points and raw means that no fitting to the experimentally-obtained data was applied. The data from

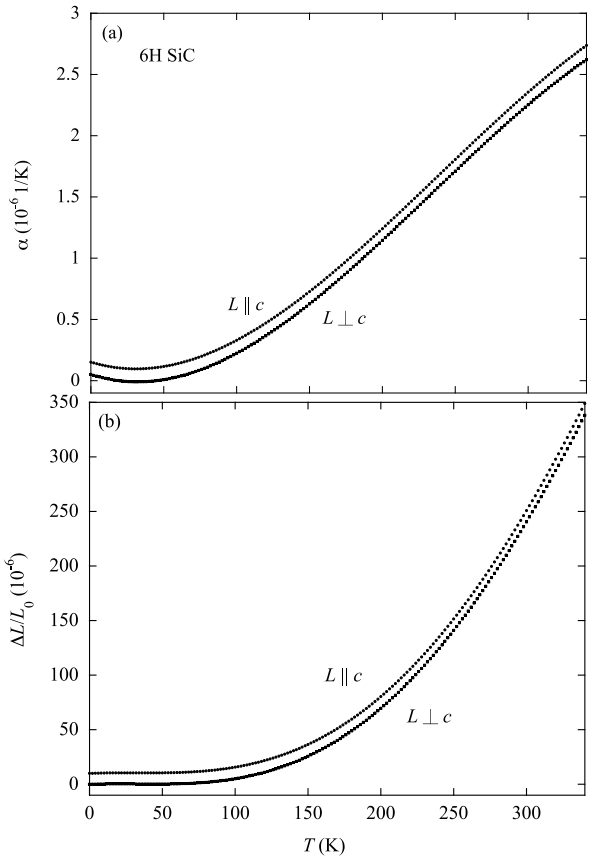

Fig. 3. Thermal expansion data for 6H SiC. (a) Thermal expansion coefficient α versus T. The $L \parallel c$ data are shifted upward by 0.1×10^{-6} 1/K for clarity. (b) Linear thermal expansion $\Delta L/L_0$ versus T. The $L \parallel c$ data are shifted upward by 10×10^{-6} for clarity.

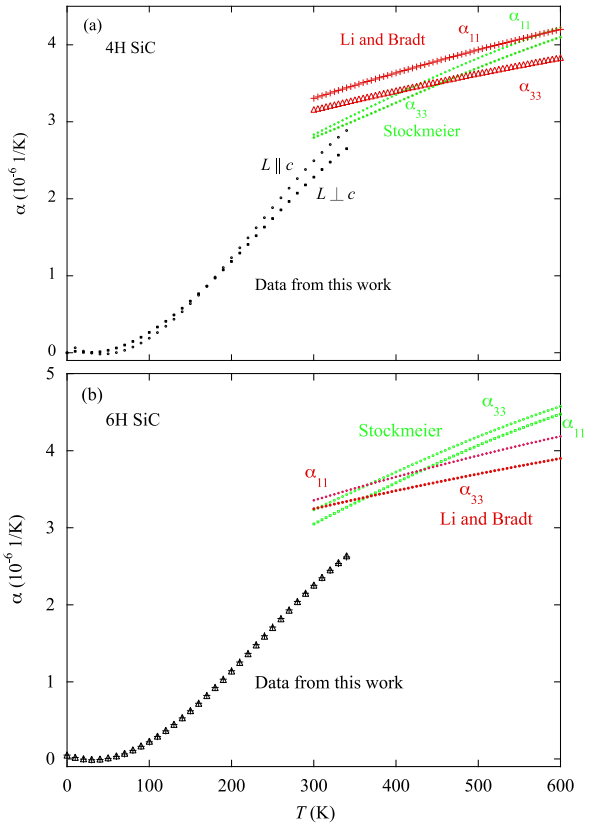

Fig. 4. (a) Thermal expansion coefficient α versus T data for 4H SiC from the present work plotted together with data from Refs. [11,13]. Data points were calculated at 5 K intervals using the fit equations provided in those reports. (b) Thermal expansion coefficient α versus T data for 6H SiC from the present work plotted together with data from Refs. [12,13]. Data points were calculated at 5 K intervals using the fit equations provided in those reports.

Ref. [12] were obtained by digitizing the data from that work, since it was not tabulated. Immediately apparent is the excellent agreement in the general behavior of the data from the two different types of measurements. More specifically, the slope of the $\Delta L/L_{294}$ data appears as if its trend is such that it agrees well with the $\Delta c/c_{294}$ data in the region immediately above 294 K. However, the scatter in the $\Delta c/c_{294}$ data is large when compared to the $\Delta L/L_{294}$ data. Fitting $\Delta c/c_{294}$ to a straight line, which seems reasonable from a visual inspection, yields $\alpha = 4.20(9) \times 10^{-6}$ 1/K, reflecting an uncertainty smaller than the estimate stated in the paragraph above; fitting with 2nd-, or 3rd-order polynomials improves the fit quality minimally (R-values from 0.99770 to 0.99930, and 0.99929, respectively). Thus, the considerations in this and the preceding paragraph, and the large value of $\alpha = 4.20(9) \times 10^{-6}$ 1/K compared to the values reported herein, lead us to conclude that the thermal expansion coefficients from lattice parameter studies are in disagreement with those of the present work due to the better resolution of capacitive dilatometry in determining α, which is well known [23].

In the absence of phase transitions, the thermal expansion of solids is associated with anharmonicity in the electrostatic potentials between neighboring atoms [23]. Anisotropic crystal structures will naturally possess anisotropies in those potentials, which could lead to anisotropy in the thermal expansion. Hexagonal crystal structures fall into this category, and they often exhibit anisotropic thermal expansion [25]. The crystal structure of 4H SiC consists of an equal number of cubic and hexagonal bonds [26,27], with stacking sequences of ABCB. The crystal structure of 6H SiC consists of two-thirds cubic bonds and one-third hexagonal bonds [26,27] with stacking sequences of ABCACB. Thus, the smaller anisotropy of 6H SiC, when compared to 4H SiC, can be

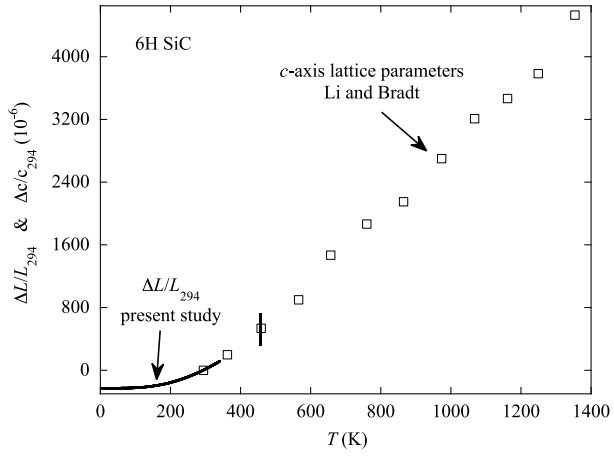

Fig. 5. Linear thermal expansion $\Delta L/L_{294}$ ($L \parallel c$) versus T from the present study plotted together $\Delta c/c_{294}$ versus T from Ref. [12] for 6H SiC. The vertical line on the single open square reflects the stated uncertainty for the lattice parameter data. The $\Delta L/L_{294}$ data are the raw data from the experiment; 1869 data points are plotted.

understood as a result of the higher ratio of cubic bonds in the former [9]. These structural differences are illustrated in Fig. 6, where the Si-C layers with a cubic environment have the Si atoms in red and the layers with an hexagonal environment have the Si atoms in yellow. Evident is the fact that the 4H structure (on the left) has 2 out of 4 red layers in the unit cell, while the 6H structure (on the right) has 4 out of 6 layers that

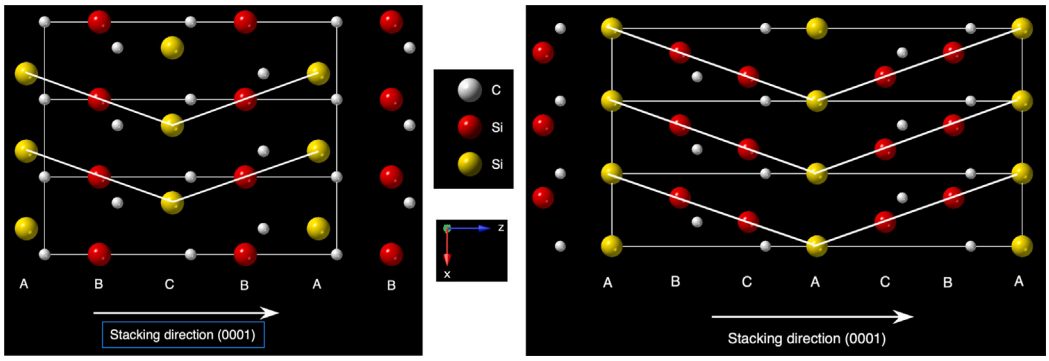

Fig. 6. Crystal structures of 4H-SiC (left panel) and 6H-SiC (right panel) showing the stacking sequence of Si-C layers along the c-axis direction, ABCB for 4H and ABCACB for 6H. The stacking sequence difference results in half of the sites in Si-C layers residing in a cubic environment for 4H and two-thirds of the Si-C layers residing in a cubic environment for 6H. The layers in a cubic environment are shown with red color while the layers with sites in an hexagonal environment are shown in yellow. Although there are three inequivalent crystal sites for Si in 6H-SiC, the coloring scheme only differentiates between cubic and hexagonal sites.

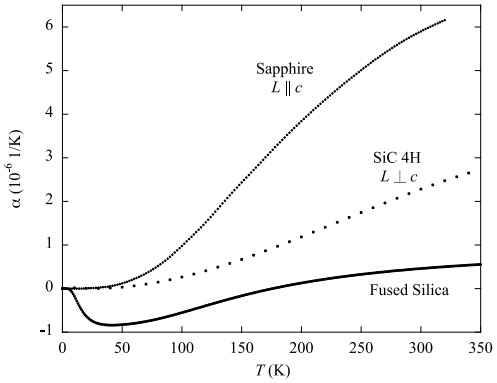

Fig. 7. Comparison of the thermal expansion coefficients of fused silica, sapphire (along the a axis), and 4H SiC ($L \perp c$).

are red in the unit cell. So 1/2 versus 2/3 layers in cubic environment. A line connecting the Si atoms in the figure illustrates that stacking is staggered along (0001) but the sequence breaks (changes direction) always at the yellow Si atoms (the hexagonal-environment sites).

The thermal expansions of 4H and 6H SiC are extremely small. This is illustrated in Fig. 7, where the thermal expansion coefficients of 4H SiC, sapphire [19], and fused silica [20,21] are plotted. Note that the α for 6H SiC is very similar to 4H SiC, and is therefore omitted from the plot. Fused silica has among the smallest known thermal expansion coefficients in the region from 30 K < T < 300 K. Sapphire has an exceptionally small thermal expansion coefficient below 100 K as well [19]. Besides the small α values observed for 4H and 6H SiC, the data in Fig. 7 also illustrate that α is very well behaved, unlike fused silica where a minimum is observed since α changes sign twice and reaches a large magnitude near 40 K. This observation could be important for low-temperature applications where a material with very well behaved thermal expansion is required. SiC may be an ideal candidate for such applications, especially given its wide availability.

6. Conclusions

The thermal expansion of the 4H and 6H polytypes of SiC for the region below room temperature is reported for the first time. The thermal expansion coefficient α of 4H SiC is slightly anisotropic for measurements parallel and perpendicular to the crystallographic c axis with $\alpha^{\parallel}$ about 2×10^{-7} 1/K larger than $\alpha^{\perp}$ near room temperature. For 6H SiC no discernible anisotropy is observed. The differences in anisotropy can be understood by considering the ratio of hexagonal to cubic bonds of each polytype. The thermal expansion coefficient is below 3×10^{-6} 1/K near room temperature for both polytypes, which is smaller than discerned from lattice parameter measurements. The discrepancy is attributed to the significantly higher relative resolution of the dilatometry technique used here. No phase transitions are observed over the range of the measurements. Tabulated data, polynomial fits, and fit parameters are provided to enable readers to easily use the data presented here in future research and technological applications of SiC.

CRediT authorship contribution statement

J.J. Neumeier: Executed all measurements, Conducted data analysis, Wrote, Edited, Submitted the manuscript. **Yu.V. Shvyd'ko:** Conceptualized the project, Provided samples and supplies, Produced figure of 4H and 6H structures, Edited manuscript. **D. Haskel:** Conceptualized the project, Provided samples and supplies, Produced figure of 4H and 6H structures, Edited manuscript.

Declaration of competing interest

The authors declare the following financial interests/personal relationships which may be considered as potential competing interests: John J. Neumeier reports financial support was provided by Montana State University.

Data availability

All data are provided in tabulated fashion within the article.

Acknowledgments

Work at Argonne was supported by the U.S. DOE Office of Science, Office of Basic Energy Sciences, under Award No. DE-AC02-06CH11357. We thank Dr. XianRong Huang for advice on sourcing 4H commercial wafers and for wire cutting them.

Appendix. Tabulated data, fit parameters, comparisons to fused silica and sapphire

A.1. Tabulated data

See Tables A.1 and A.2.

A.2. Fit parameters

The parameters obtained from fitting the $\alpha(T)$ data to Eq. (1) are provided in Table A.3.

Table A.1
Thermal expansion data for 4H SiC perpendicular (⊥) and parallel (||) to the c axis.[a]

T (K)	$\Delta L_{\perp}/L_0$ (10^{-6})	$\Delta L_{\|\|}/L_0$ (10^{-6})	$\alpha_{\perp}$ (10^{-6} K^{-1})	$\alpha_{\|\|}$ (10^{-6} K^{-1})	$\Delta V/V_0$ (10^{-6})	β (10^{-6}K^{-1})
0	0	0	0	0	0	0
10.0	0.288	0.932	0.018	0.065	1.508	0.1013
20.0	0.399	1.361	0.006	0.023	2.160	0.03383
30.0	0.442	1.445	0.004	−0.004	2.328	0.004593
40.0	0.525	1.338	0.014	−0.016	2.388	0.01177
50.0	0.753	1.188	0.033	−0.013	2.694	0.05360
60.0	1.224	1.134	0.062	0.004	3.583	0.1282
70.0	2.033	1.309	0.101	0.033	5.375	0.2339
80.0	3.266	1.838	0.147	0.074	8.370	0.3687
90.0	5.008	2.836	0.202	0.127	12.85	0.5309
100	7.335	4.414	0.264	0.190	19.08	0.7187
110	10.32	6.673	0.334	0.263	27.32	0.9303
120	14.03	9.707	0.409	0.345	37.77	1.164
130	18.53	13.60	0.491	0.435	50.67	1.417
140	23.88	18.44	0.578	0.533	66.19	1.689
150	30.12	24.29	0.670	0.637	84.52	1.978
160	37.30	31.21	0.767	0.748	105.8	2.281
170	45.46	39.26	0.867	0.863	130.2	2.597
180	54.65	48.49	0.971	0.984	157.8	2.925
190	64.88	58.94	1.077	1.107	188.7	3.261
200	76.20	70.65	1.185	1.234	223.0	3.605
210	88.60	83.63	1.296	1.363	260.8	3.955
220	102.1	97.91	1.407	1.493	302.1	4.308
230	116.8	113.5	1.520	1.624	347.0	4.664
240	132.5	130.4	1.632	1.755	395.4	5.019
250	149.4	148.6	1.744	1.885	447.4	5.373
260	167.4	168.1	1.856	2.013	502.9	5.724
270	186.5	188.8	1.966	2.139	561.8	6.070
280	206.7	210.8	2.074	2.261	624.2	6.408
290	228.0	234.0	2.179	2.380	690.0	6.738
300	250.3	258.4	2.282	2.494	759.0	7.057
310	273.6	283.9	2.381	2.602	831.1	7.364
320	297.9	310.4	2.476	2.705	906.2	7.656
330	323.1	338.0	2.566	2.800	984.1	7.932
340	349.2	366.4	2.652	2.887	1065	8.191

[a] The uncertainties of the $\Delta L_{\perp}/L_0$, α, $\Delta V/V_0$, and β values are approximately 2×10^{-8}, 2×10^{-8} 1/K, 4×10^{-8}, and 4×10^{-8} 1/K, respectively.

Table A.2
Thermal expansion data for 6H SiC perpendicular (⊥) and parallel (||) to the c axis.[a]

T (K)	$\Delta L_{\perp}/L_0$ (10^{-6})	$\Delta L_{\|\|}/L_0$ (10^{-6})	$\alpha_{\perp}$ (10^{-6} K^{-1})	$\alpha_{\|\|}$ (10^{-6} K^{-1})	$\Delta V/V_0$ (10^{-6})	β (10^{-6} K^{-1})
0	0	0	0	0	0	0
10.0	0.340	0.355	0.018	0.021	1.034	0.058
20.0	0.416	0.466	−0.002	0.003	1.298	−0.001
30.0	0.351	0.454	−0.010	−0.004	1.156	−0.023
40.0	0.265	0.430	−0.006	0.001	0.959	−0.0121
50.0	0.267	0.503	0.008	0.015	1.036	0.032
60.0	0.464	0.775	0.033	0.040	1.703	0.106
70.0	0.957	1.345	0.067	0.075	3.259	0.209
80.0	1.841	2.304	0.111	0.118	5.985	0.340
90.0	3.204	3.738	0.163	0.170	10.146	0.496
100	5.131	5.730	0.223	0.230	15.991	0.676
110	7.698	8.355	0.291	0.296	23.752	0.879
120	10.98	11.68	0.366	0.370	33.643	1.102
130	15.04	15.78	0.447	0.450	45.863	1.344
140	19.94	20.71	0.534	0.536	60.595	1.604
150	25.74	26.52	0.626	0.627	78.003	1.879
160	32.48	33.27	0.723	0.723	98.235	2.169
170	40.22	40.99	0.824	0.823	121.42	2.471
180	48.98	49.73	0.929	0.926	147.69	2.783
190	58.80	59.52	1.036	1.033	177.12	3.105
200	69.70	70.39	1.146	1.142	209.80	3.433
210	81.72	82.36	1.258	1.253	245.81	3.768
220	94.86	95.45	1.371	1.365	285.18	4.106
230	109.1	109.7	1.484	1.479	327.94	4.447
240	124.5	125.0	1.598	1.593	374.13	4.789
250	141.1	141.5	1.712	1.706	423.72	5.130
260	158.8	159.2	1.824	1.820	476.71	5.468
270	177.6	177.9	1.935	1.932	533.06	5.802

(*continued on next page*)

Table A.2 (*continued*).

T (K)	$\Delta L_{\perp}/L_0$ (10^{-6})	$\Delta L_{\|\|}/L_0$ (10^{-6})	$\alpha_{\perp}$ (10^{-6} K^{-1})	$\alpha_{\|\|}$ (10^{-6} K^{-1})	$\Delta V/V_0$ (10^{-6})	β (10^{-6} K^{-1})
280	197.5	197.8	2.044	2.042	592.72	6.129
290	218.4	218.7	2.150	2.150	655.62	6.450
300	240.5	240.8	2.253	2.255	721.68	6.761
310	263.5	263.8	2.352	2.357	790.79	7.061
320	287.5	287.9	2.446	2.455	862.84	7.348
330	312.4	312.9	2.536	2.549	937.70	7.621
340	338.2	338.9	2.620	2.638	1015.2	7.878

[a] The uncertainties of the $\Delta L_{\perp}/L_0$, α, $\Delta V/V_0$, and β values are approximately 2×10^{-8}, 2×10^{-8} 1/K, 4×10^{-8}, and 4×10^{-8} 1/K, respectively.

Table A.3
Fit parameters for $\alpha(T) = A + BT + C(2T^2 - 1) + D(4T^3 - 3T)$ (K^{-1}) (5 K < T < 340 K).

Parameter	Si-4H		Si-6H	
	$\perp c$	$\|\| c$	$\perp c$	$\|\| c$
A	$4.22(26) \times 10^{-8}$	$1.245(58) \times 10^{-7}$	$5.11(24) \times 10^{-8}$	$5.15(52) \times 10^{-8}$
B	$-3.020(55) \times 10^{-9}$	$-6.78(14) \times 10^{-9}$	$-3.916(59) \times 10^{-9}$	$-3.66(12) \times 10^{-9}$
C	$3.057(17) \times 10^{-11}$	$4.353(48) \times 10^{-11}$	$3.291(20) \times 10^{-11}$	$3.167(38) \times 10^{-11}$
D	$-2.183(15) \times 10^{-14}$	$-3.178(46) \times 10^{-14}$	$-2.358(19) \times 10^{-14}$	$-2.220(35) \times 10^{-14}$
χ^2	7.02×10^{-13}	2.29×10^{-11}	3.18×10^{-12}	1.52×10^{-11}

References

[1] E. Papanasam, B.P. Kumar, B. Chanthini, E. Manikandan, L. Agarwal, A comprehensive review of recent progress, prospect and challenges of silicon carbide and its applications, Silicon 14 (18) (2022/12/01) 12887–12900, http://dx.doi.org/10.1007/s12633-022-01998-9.

[2] D. Fang, W. Li, T. Cheng, Z. Qu, Y. Chen, R. Wang, S. Ai, Review on mechanics of ultra-high-temperature materials, Acta Mech. Sin. 37 (9) (2021) 1347–1370, http://dx.doi.org/10.1007/s10409-021-01146-3.

[3] N.D. Andraskar, G. Tiwari, M.D. Goel, Impact response of ceramic structures - A review, Ceram. Int. 48 (19, A) (2022) 27262–27279, http://dx.doi.org/10.1016/j.ceramint.2022.06.313.

[4] Z. Sun, X. Chen, Y. Mao, L. Zhang, J. Feng, Joining of SiC ceramics using CaO-Al2O3-SiO2 (CAS) glass ceramics, J. Eur. Ceram. 40 (2) (2020) 267–275, http://dx.doi.org/10.1016/j.jeurceramsoc.2019.09.030, URL https://www.sciencedirect.com/science/article/pii/S0955221919306405.

[5] O. Qin, W. Yanfei, X. Jian, L. Yinsheng, P. Xueliang, M. Gaoming, L. Mian, L. Peng, Z. Xiaobing, G. Fangfang, Z. Chonghong, H. Liu, Y. Lei, H. Zhengren, C. Zhifang, Z. Wenlong, H. Qing, Research progress of SiC fiber reinforced SiC composites for nuclear application, J. Inorg. Mater. 37 (8) (2022) 821–840, http://dx.doi.org/10.15541/jim20220145.

[6] T.D.P.V. Jalluri, S. Somashekar, A. Dey, R. Venkateswaran, S. Elumalai, B. Rudraswamy, K.V. Sriram, Characterization of thermal sprayed si on sintered SiC for space optical applications, Surf. Eng. 37 (5) (2021) 558–571, http://dx.doi.org/10.1080/02670844.2020.1803718, arXiv:https://doi.org/10.1080/02670844.2020.1803718.

[7] P. Gloesener, F. Wolfs, M. Cola, E. Wachtelaer, C. Flebus, Optics for EUCLID telescope: challenges and developments, in: R. Navarro, R. Geyl (Eds.), Advances in Optical and Mechanical Technologies for Telescopes and Instrumentation IV, Vol. 11451, International Society for Optics and Photonics, SPIE, 2020, p. 114510L, http://dx.doi.org/10.1117/12.2562807.

[8] W.F. Koehl, B.B. Buckley, F.J. Heremans, G. Calusine, D.D. Awschalom, Room temperature coherent control of defect spin qubits in silicon carbide, Nature 479 (7371) (2011/11/01) 84–87, http://dx.doi.org/10.1038/nature10562.

[9] A. Lebedev, Heterojunctions and superlattices based on silicon carbide, Semiconduct. Sci. Technol. 21 (2006) R17, http://dx.doi.org/10.1088/0268-1242/21/6/R01.

[10] J. Strempfer, S. Kearney, A. Khan, D. Capatina, R. Reininger, D. Shu, C. Wolford, M. Golebiowski, L. Rebuffi, X. Shi, T. Kołodziej, X. Huang, Y. Shvyd'ko, Y. Choi, G. Fabbris, I. Kesgin, Y. Ivanyushenkov, E. Gluskin, D. Haskel, Possibilities at the polar beamline with APS-U, J. Phys. Conf. Ser. 2380 (1) (2022) 012038, http://dx.doi.org/10.1088/1742-6596/2380/1/012038, URL https://doi.org/10.1088/1742-6596/2380/1/012038.

[11] Z. LI, R. Bradt, Thermal-expansion of the hexagonal (H-4) polytype of SiC., J. Appl. Phys. 60 (2) (1986) 612–614, http://dx.doi.org/10.1063/1.337456.

[12] Z. Li, R. Bradt, Thermal expansion of the hexagonal (6H) polytype of silicon carbide, J. Amer. Ceram. Soc. 69 (12) (1986) 863–866.

[13] M. Stockmeier, R. Müller, S.A. Sakwe, P.J. Wellmann, A. Magerl, On the lattice parameters of silicon carbide, J. Appl. Phys. 105 (3) (2009) 033511, http://dx.doi.org/10.1063/1.3074301, arXiv:https://doi.org/10.1063/1.3074301.

[14] J.J. Neumeier, R.K. Bollinger, G.E. Timmins, C.R. Lane, R.D. Krogstad, J. Macaluso, Capacitive-based dilatometer cell constructed of fused quartz for measuring the thermal expansion of solids, Rev. Sci. Instrum. 79 (3) (2008) 033903, http://dx.doi.org/10.1063/1.2884193, arXiv:https://doi.org/10.1063/1.2884193.

[15] B. Brito, G.-Q. Hai, L. Cândido, Isotopic effect on thermal physical properties of cubic SiC, Comput. Mater. Sci. 226 (2023) 112244, http://dx.doi.org/10.1016/j.commatsci.2023.112244, URL https://www.sciencedirect.com/science/article/pii/S0927025623002380.

[16] E.H. Abdul-Hafidh, The prediction of the bulk modulus and its temperature-derivative of the crystalline SiC ceramic, Silicon (2023/04/19) http://dx.doi.org/10.1007/s12633-023-02461-z.

[17] H. Sakakima, S. Takamoto, A. Hatano, S. Izumi, Temperature-dependent stacking fault energies of 4H-SiC: A first-principles study, J. Appl. Phys. 127 (12) (2020) 125703, http://dx.doi.org/10.1063/1.5141029, arXiv:https://pubs.aip.org/aip/jap/article-pdf/doi/10.1063/1.5141029/15244885/125703_1_online.pdf.

[18] P. Prajapat, D.K. Singh, G. Gupta, Growth of III-nitrides by molecular beam epitaxy: Unconventional substrates for conventional semiconductors, Mater. Sci. Eng. B: Solid-State Mater. 295 (2023) 116574, http://dx.doi.org/10.1016/j.mseb.2023.116574, URL https://www.sciencedirect.com/science/article/pii/S0921510723003161.

[19] J.J. Neumeier, G.A. Nelson, Sapphire dilatometer cell for measuring the thermal expansion of solids, Rev. Sci. Instrum. 93 (6) (2022) 063903, http://dx.doi.org/10.1063/5.0091377, arXiv:https://pubs.aip.org/aip/rsi/article-pdf/doi/10.1063/5.0091377/16632284/063903_1_online.pdf.

[20] M. Okaji, A precision interferometric dilatometer by means of optical heterodyne interferometry, Netsubussei 6 (1992) 83–88.

[21] M. Okaji, N. Yamada, K. Nara, H. Kato, Laser interferometric dilatometer at low temperatures: application to fused silica SRM 739, Cryogenics 35 (12) (1995) 887–891, http://dx.doi.org/10.1016/0011-2275(95)96887-R, URL https://www.sciencedirect.com/science/article/pii/001122759596887R.

[22] F.R. Kroeger, C.A. Swenson, Absolute linear thermal expansion measurements on copper and aluminum from 5 to 320 K, J. Appl. Phys. 48 (3) (1977) 853–864, http://dx.doi.org/10.1063/1.323746, arXiv:https://doi.org/10.1063/1.323746.

[23] T.H.K. Barron, J.G. Collins, G.K. White, Thermal expansion of solids at low temperatures, Adv. Phys. 29 (4) (1980) 609–730.

[24] R. Suleimanov, N. Abdullaev, The nature of negative linear expansion of graphite crystals, Carbon 31 (7) (1993) 1011–1013, http://dx.doi.org/10.1016/0008-6223(93)90050-K, URL https://www.sciencedirect.com/science/article/pii/000862239390050K.

[25] T.H.K. Barron, G.K. White, Heat Capacity and Thermal Expansion At Low Temperatures, Kluwer, New York, 1999.

[26] G.R. Fisher, P. Barnes, Toward a unified view of polytypism in silicon carbide, Phil. Mag. 61 (2) (1990) 217–236.

[27] P. Bechstedt, P. Käckell, A. Zywietz, K. Karch, B. Adolph, K. Tenelsen, J. Furthmüller, Polytypism and properties of silicon carbide, Phys. Status Solidi b 202 (1) (1997) 35–62.